Peculiarities of the aerosol vertical distribution during the passage of dust storms over the Peter the Great Bay in 2006 and their influence on phytoplankton communities in the Japan Sea

O.A. Bukin,[1] A.N. Pavlov,[2] P.A. Salyuk,[1] Yu.N. Kulchin,[2] K.A. Shmirko,[1] S.Yu. Stolyarchuk,[3] and A.Yu. Bubnovskii[1]

[1] *V.I. Il'ichev Pacific Institute of Oceanology, Far Eastern Branch of the Russian Academy of Sciences,*
[2] *Institute of Automation and Control Processes, Far Eastern Branch of the Russian Academy of Sciences,*
[3] *G.I. Nevel'ski Marine State University, Vladivostok*

We present results of the study of atmospheric aerosol structure and influence of aerosol on the activity of phytoplankton communities in different areas of Japan Sea during the most intense dust storms in Gobi dessert (from March to June, 2006). The joint analysis of lidar sounding and Aqua/MODIS data has revealed typical stratifications of the tropospheric aerosol during the dust storms. The results obtained agree with the theoretical computations. The altitude of aerosol localization is determined and the increase of chlorophyll «A» concentration is recorded due to aerosol matter export to the upper layer of the ocean over the areas under study.

Introduction

Atmospheric aerosol not only plays an essential role in climate formation, but is one of the factors that influence the activity of photosynthetic structures in the ocean. This influence results directly from the export of huge amount of mineral substances from the mainland to the photic ocean layer (which leads to local bloom on the aerosol exposed areas) and changes of albedo and spectrum of solar radiation reaching the sea surface.

Some continental aerosol, exported to the atmosphere after dust storms or volcanic eruptions, is localized at the altitudes where temperature profile of the atmosphere has peculiar features and can reside there for a long time.[1-3] Aerosol masses, trapped within the height regions with sharp temperature gradients, can be transported at long distances under the action of wind. Thus, aerosol, exported by dust storms in Sahara dessert, is observed over the Atlantic Ocean and reaches coasts of America.[4,5] While being transported, across the Atlantics apportion of aerosol falls down to the ocean thus increasing the concentration of microelements in the surface layer of the ocean (SLO). This increase of concentration (particularly, of iron, silicon, and phosphorus), even small, can cause local bloom of the phytoplankton and significant increase of the chlorophyll "A" concentration.[6-8]

The complexity of the study of aerosol transportation and peculiarities of its influence on phytoplankton communities is caused by large spatial and temporal scales of the phenomena, the necessity to measure the parameters directly characterizing aerosol transport as well as the corresponding response of a phytoplankton community. Nevertheless, there are papers describing such studies in detail, e.g., Refs. 4–6. Note, that one of the tasks of the lidar networks in aerosol-exposed regions (EARLiNet, ADNet, CISLiNet) is the monitoring of the dust outburst from Sahara and Gobi desserts sand storms, and their influence on the sea ecosystems.[9-11]

Strong dust storms in continental areas of China and Mongolia can be considered not only as a climate-forming factor in Asia but as a process deeply influencing the functioning of phytoplankton communities in waters of marginal sea of the western part of the Pacific ocean, i.e., the East China sea, Japan sea, and the Sea of Okhotsk. Maximum north-eastward and eastward aerosol exports are observed since March until June and reaches the Kamchatka peninsula and coasts of California, respectively.[12,13] Since phytoplankton plays a key role in life support processes on the Earth, the study of responses of the phytoplankton communities to aerosol exported from mainland is of great importance.

In this paper, some peculiarities of aerosol distribution in the atmosphere and its influence on the chlorophyll "A" concentration fields are presented, which were revealed from the analysis of satellite and lidar data for the period of maximum aerosol activity (March–June, 2006) in the sea areas chosen.

1. Description of experimental data

In our analysis we have made use of the data on aerosol obtained at the lidar station in Vladivostok, and satellite data on the parameters of atmospheric aerosol and chlorophyll "A" concentration. In our comparative analysis we have used measurement data on aerosol optical depth (AOD) of the atmosphere

and data on chlorophyll "A" concentration obtained with a MODIS-Aqua scanner of the sea surface color over the observation period. Near-shore location of the lidar station allows us to study the transport of aerosol cloud from continental regions of China over the Peter the Great Bay. In addition, data on vertical distributions of humidity, temperature, and pressure, obtained with radiosondes launched every 12 hours from the site 5 km far from the lidar,[14] were used in the analysis. Data on temperature and pressure were used in calculating vertical profiles of molecular light scattering and in estimating stability of the aerosol layers.

Single-frequency laser sensing at 532 nm wavelength was carried out at day and nighttime along a slant path over the Peter the Great Bay area (zenith sensing angle equaled 50°). The description of lidar can be found in Ref. 15.

Two regions were chosen for the analysis. The first one (Fig. 1*a*) is the sea area of the Peter the Great Bay just near the lidar station, where the comparative analysis of the data on atmospheric aerosol obtained with lidar sensing and satellite measurement data on aerosol parameters was carried out. For the second region (a part of shelf of Japan sea, Fig. 1*b*), only satellite data on AOD and chlorophyll "A" concentration were compared.

a

b
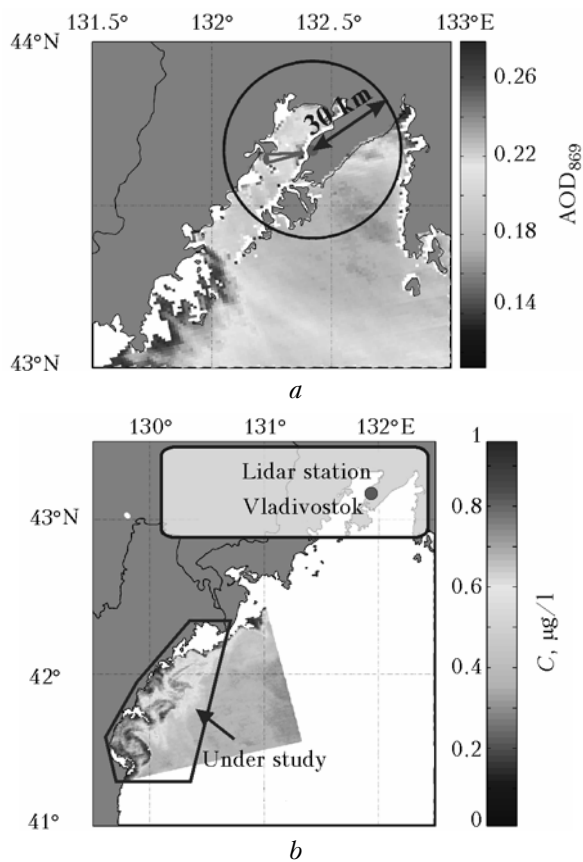
Fig. 1. Location of the lidar station superimposed on the image of the atmospheric optical depth distribution (*a*) and the chlorophyll "A" concentration distribution according to Aqua/MODIS data (*b*).

Average values of optical depth of the atmosphere and chlorophyll "A" concentration measured from satellite were obtained by averaging over image pixels within the water area circle of 30-km radius (see Fig. 1*a*) and within the second region (Fig. 1*b*).

The averaging procedure consisted in finding the arithmetic mean AOD or chlorophyll "A" concentration over all informative pixels (after corresponding filtration of the initial data).

The second region was located in the eastward direction of the Gobi aerosol transport. It was chosen because phytoplankton communities in this area undergo less influence of terrigenous factors (other than aerosol transported from mainland) compared with the first region. Besides, maximum number of high-quality images from MODIS-Aqua were available for this area during the period under study.

2. Aerosol stratification

To describe approaches to analysis of the correlation between the altitudes of the aerosol influx localization and peculiarities of the vertical temperature distribution we made use, as an example, vertical profiles the atmospheric temperature and aerosol. Figure 2*a* shows the temperature profile (radiosonde data on April 7, 2006, 09:00 of local time) and the results on altitude distribution of the backscattering coefficient β_a measured at the same time with the lidar at 523 nm wavelength (Fig. 2*b*).

a   *b*
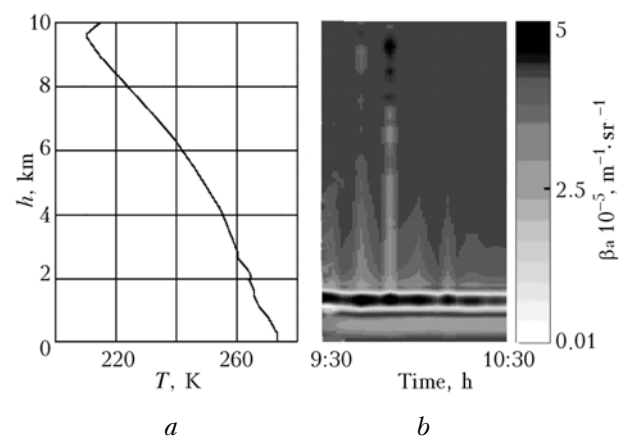
Fig. 2. Vertical distribution of temperature (radiosonde) (*a*) and backscattering coefficient (lidar) (*b*).

On this day, we have recorded the most strong aerosol influx from continental areas of China to Vladivostok (characteristic sand dust was observed in some parts of the city; during daytime and, also, heavy haze was observed above the Peter the Great Bay).

It is seen that several height regions with noticeable changes of the temperature gradient can be isolated in the temperature profile at heights to 0.5, 1.5–2.5, and 9–10 km.

It may be noted, that at least two aerosol layers correspond to these peculiarities of temperature distribution (the bottom layer at the height of 0.7 km and the layer at the height about 1 km). Large aerosol content in the bottom layer did not allow a reliable signal from the height of the third singularity of the temperature profile to be obtained on this day.

In observations of the vertical aerosol structure we have noticed that the aerosol is, as a rule, localized in several layers that may change their heights with time. The direction of vertical motions of the stratification depends on the vertical component of wind speed at the given heights. In some cases, the layer on the height of local temperature inversion experiences vertical movement. This can be caused by that the vertical temperature gradient at this height is such that the Waissala—Brent stability criterion is not fulfilled. The height range where this criterion is fulfilled and aerosol layer localization is possible can be estimated using the data on temperature profile.[16]

The Waissala—Brent frequency for free atmosphere is defined as follows[16]:

$$N^2 = -g\left(\frac{1}{\rho}\frac{\partial \rho}{\partial h} + \frac{g}{c(h)^2}\right), \tag{1}$$

where g is the gravitational acceleration, $\rho(h)$ is the atmospheric density at the height h, $c(h)$ is the speed of sound at the height h.

The vertical profile of sound speed was calculated by the formula for ideal gas, which is valid in considering the sound propagation in the atmosphere. For layers to be in the state of stable equilibrium, the following inequality must be satisfied[16]:

$$N^2 \geq 0. \tag{2}$$

Given the invariable gravitational acceleration we have calculated locations of the stable layers for temperature profiles. Figure 3 visualizes atmospheric layers (from lidar measurements) and the Waissala—Brent criterion (calculated) for May 27, 2006 when the characteristic stable three-layer structure of aerosol distribution was observed.

According to lidar data (Fig. 3a) stable aerosol layers (black color) are observed at heights up to 1 km; the stability criterion (Fig. 3b) gives similar picture in the 1.2—2.5 km range, about 4 and 10 km, i.e., dark areas 1—4 correspond to maxima exceeding the value of the stability criterion. It follows from Fig. 3, that stable layers are those localized at the heights of 0—1, 2, 4.5, and about 10 km. In other words, localization of aerosol layers over the Peter the Great Bay took place, in observation period, within the height range where the Waissala—Brent criterion fulfilled. Similar situation was observed on other days when aerosol inflow was recorded which we related to dust stormes.[17]
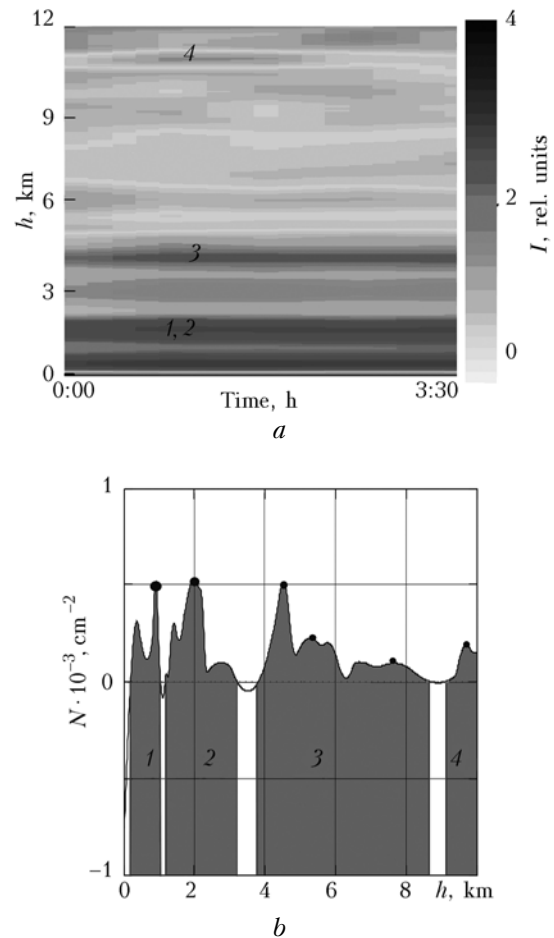
Fig. 3. Atmospheric structure on May 27, 2006. Vertical scale on the right is the relative intensity of backscattering signal in gradations of gray (a) and height of localization of stable layers (b).

3. Lidar and satellite measurements of AOD

Consider the results of lidar sensing of aerosol in the period of its intense inflow from the regions of dust storms in April—May, 2006.

The calculations of extinction profiles, backscattering coefficients, and lidar ratio were carried out by the Klett—Fernald algorithm with calibration in far-range zone. The AOD values obtained from satellite data and recalculated to the laser wavelength[18,19] were used as additional input data. In the case of no satellite data available on the days of lidar sensing, satellite AOD values were linearly interpolated. As a result, we have calculated AOD_{532} using lidar sensing data.

To account for contribution of aerosol to optical depth, the results measured in the 869-nm channel of MODIS-Aqua scanner were used. The optical depth obtained from data of this channel is free of the contribution of radiation upwelling from the sea water. Then, the data were recalculation to yield AOD at 532 nm wavelength (for comparison with lidar data) using the following equation[18]:

$$\tau_P = \tau_0(\lambda/\lambda_0)^{-m}, \qquad (3)$$

where τ_P and τ_0 are the AOD values at the wavelengths λ and λ_0; m is the Ångström coefficient for transition to the optical depth at the wavelength λ.

Temporal dynamics of AOD was analyzed in three height ranges within which AOD values were integrated. These ranges were chosen so that we could separate the layers mainly observed during the period under study. The first region from 0 to 3 km included all aerosol structures generated inside the boundary layer (in Fig. 3, layers *1* and *2* were combined). Second and third layers were within the heights of 3–5 and 5–10 km (aerosol concentrated near the tropopause was included).

Figure 4,*a* shows the time variation of AOD_{532} obtained from satellite and lidar data (in different layers) for the region under study (see Fig. 1a).

a

b
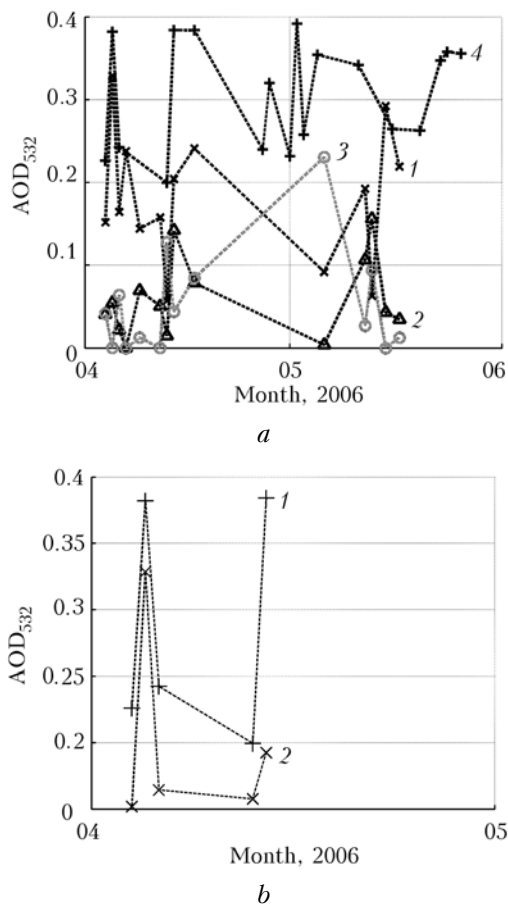
Fig. 4. Time variation of AOD_{532} in the isolated layers: *a* — AOD_{532} in 0–3 km (*1*), 3–5 km (*2*), 5–10 km (*3*), satellite data (*4*); *b* — satellite (*1*) and lidar (*2*) measurements in the 0–3 km height range on the same dates.

Maxima in the time variation of AOD correspond to the enhanced aerosol content in the atmosphere over the territory under study in the period of most intense influx from Gobi. In most cases, the dates when the maxima were observed

coincided with the dates of aerosol inflows, simulated with the account of actual meteorological information.[17]

One can note that the bulk of aerosol transported from the Gobi is localized within the planetary boundary layer, hence, maximum income of mineral matters to SLO is to be expected in these periods.

The time variation of AOD_{532} in the 0–3 km layer best of all correlates with that of integrated satellite data on AOD_{532}. Though the correlation coefficient is not large (0.4), one can say that the bulk of aerosol is transported within these heights (the coefficients of correlation between satellite and lidar AOD of other height layers are much smaller). Small correlation coefficient in this case is explained by the movement of aerosol masses and transition of suspended matter from one stratification level to another (presence of regions of autocorrelation with the satellite data).

To calculate the correlation coefficient, satellite and lidar data were interpolated on a uniform grid. Figure 4*b* shows the time variations of AOD_{532} retrieved from lidar sensing data within the planetary boundary layer and from satellite measurements for the days when satellite data were obtained together with lidar data during satellite overflight above the area under study. Small number of synchronous measurements makes the value of the correlation coefficient unreliable (0.8), but qualitative coincidence of the time variation of AOD_{532}, integrated over the atmospheric column, and AOD_{532} in the bottom layer can nevertheless, be stated for these days.

The highest AOD_{532} values were virtually always observed in the layer of turbulent mixing (or convective boundary layer[20,21]) as compared with higher layers, excluding the situation in the first half of May (see Fig. 4*a*) when the bulk of aerosol was located near the tropopause.

It is necessary to note that the highest values of AOD_{532} in the bottom layer were recorded on April 7 and in the period from April 10 to 17 when most intense aerosol influx to the atmosphere over the Peter the Great Bay from the continental areas of China was observed. The noted characteristic feature of the tropospheric aerosol (see Fig. 4*a*) is its dynamical redistribution between stratification levels. Indeed, the decrease of AOD_{532} in some layers results in its increase in other layers while the integral aerosol optical depth is free from that significant fluctuations according to satellite data.

4. Aerosol influence on phytoplankton communities

The algae blooming consists in sharp increase of the phytoplankton cells concentration (chlorophyll "A" concentration), depends on many factors, and manifests itself differently in different climate zones of the Pacific ocean. In the Japan sea, spring bloom

begins in March and lasts until the end of May. Thus, transport of sand storm aerosol to the areas of marginal seas of the western part of the Pacific ocean falls just on the period of spring bloom. Extra local bloom due to the mineral substances from the mainland must manifest itself against the background of spring bloom.

Despite the fact that blooming is delayed with respect to the income of mineral substances, correlation between these two processes has to be observed. The question on how quickly a phytoplankton community responds to the inflow of mineral substances to SLO is yet poorly studied. The dependence of phytoplankton response to an external action on the conditions where cells development takes place, on the stage of the development, species composition, and type of the processes can be assumed. As was shown in Refs. 22 and 23, where the response of phytoplankton communities to the influence of hurricanes was studied, the maximum increase of chlorophyll "A" concentration is observed approximately in a week after a typhoon. Sharp increase of chlorophyll "A" concentration was observed[7] two days after the dispersion of iron salts over the area under study. Apparently, active mixing of the surface layer by a typhoon and change in hydrological, geochemical, and other seawater parameters affect the activity of a photosynthetic system in a way different than the growth of the electron transport rate in the photosynthesis reaction, which occurs at the increase of iron concentration in seawater. A number of studies considering the response of phytoplankton to the influence of dust storms do not allow even approximate estimation of the time interval when phytoplankton cells begin to react to aerosol influx. Such studies could be of undoubted interest.

Figure 5 shows the results on reconstructed chlorophyll "A" concentration and atmospheric optical depth for the two above-mentioned regions.

For the first region (see Fig. 1a), the time variation of chlorophyll "A" concentration, reconstructed from MODIS-Aqua data, was compared with the time variation of AOD_{532} in the 0–3 km height range obtained from lidar sensing (Fig. 5a). For the second region (see Fig. 1b), the comparison with the time variation of AOD_{869} (MODIS-Aqua) was carried out in view of lack of lidar data. The corresponding cross-correlation functions for both regions are shown in Fig. 6. Maximum correlation coefficients for the first and second regions are 0.5 and 0.6 when shifting the time variation of chlorophyll "A" concentration left to 80 and 40 h, respectively. This evidences of the correlation between aerosol influx to the atmosphere over the areas under study and the increase of chlorophyll "A" concentration.

It is necessary to note, that algae blooming (global spring bloom) proceeds in markedly different way in the first and second regions. In the second region (open shelf waters, see Fig. 1b), the spring bloom proceeds following the "classical" scenario,

i.e., monotonic concentration increase from March to the end of May and following decrease in June.
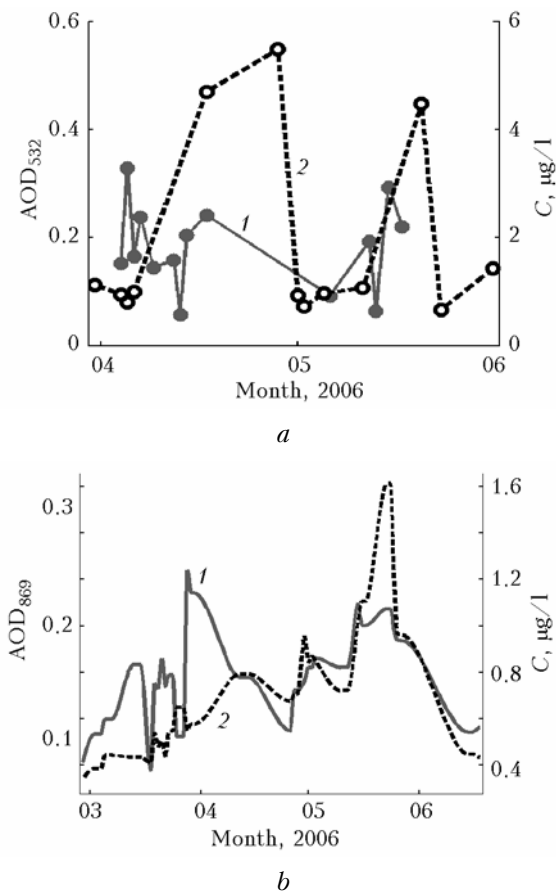
Fig. 5. Time variations: a – AOD_{532} (lidar) (curve 1) and chlorophyll "A" concentration (MODIS) (curve 2) in the first region; b – AOD_{869} (MODIS) (curve 1) and chlorophyll "A" concentration (MODIS) (curve 2) in the second region.

The peculiarities of the first region (see Fig. 1a) are its relative closure from the waters of the Japan sea and strong influence of anthropogenic factors and income of terrigenous material from rivers flowing into it on algae blooming. This makes the peak of spring bloom less pronounced in comparison with the second region and approximately stable chlorophyll "A" concentration during the bloom. Against this global bloom, local concentration increases are noticeable, which can be related to aerosol inflow events. These events can increase the concentration of elements limiting phytoplankton development, e.g., iron[7,8]; in this case, the maximum of the cross correlation function is achieved when time variation of chlorophyll "A" concentration is shifted to the left by 80 h for the first region and 40 h for the second one (see Fig. 6), i.e., according to our assessments, the reaction of phytoplankton to aerosol inflow amounts to 2–3 days. This agrees with experimental data[4,7] on phytoplankton reaction to adding iron into seawater.
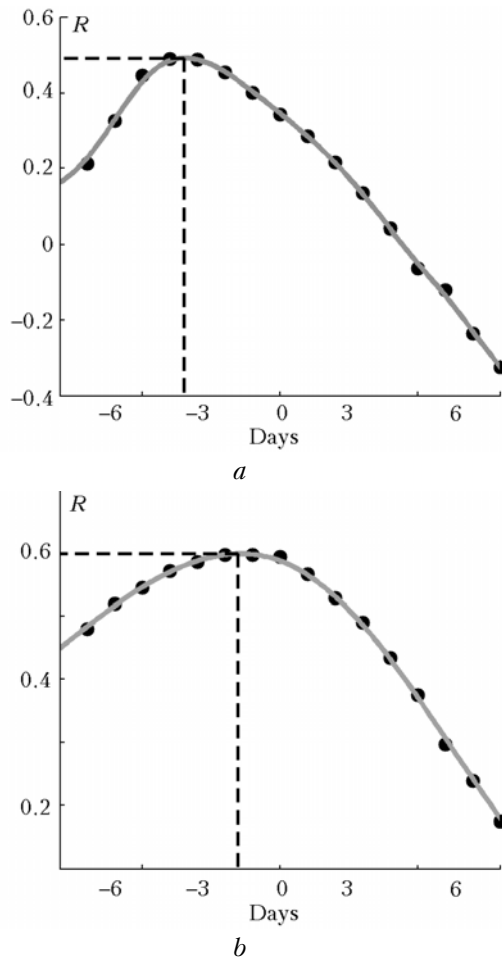
Fig. 6. Correlation coefficient as a function of the shift of time variation of chlorophyll "A" concentration in the first (*a*) and second (*b*) regions.

Eastward aerosol transport (toward the second region under study) from the continental China in the period from March to June was more complicated. This is explained by the fact that main aerosol inflow occurs along this direction and virtually constantly, during dust storms.[17] If for the north-eastward direction only three periods can be isolated of the AOD increase in the low layer up to 3 km in the 0−3 km layer, then for the eastward transport such events were observed much more frequently. It is possible that the "classical" course of blooming is mainly determined by aerosol deposition to SLO in this region, as AOD increasing from March to June demonstrates a monotonic behavior similar to that of chlorophyll "A" concentration against which sharp concentration increases are observed correlated with the sharp increases of AOD.

Conclusion

The proposed three-layer structure of aerosol vertical distribution is evidently characteristic of the region in the period of dust storms and is convenient for describing the processes of aerosol transport and its influence on the phytoplankton communities. Layering of the troposphere (0−3, 3−5, and 5−10 km) is quite acceptable for this region, as it allows estimating not only the part of aerosol, localized in the bottom layer and potentially directly influences the functioning of phytoplankton cells, but also aerosol, localized in free atmosphere and near the tropopause, which influences phytoplankton communities indirectly. These layers are relatively stable and are localized at the heights of local temperature inversions, where the stability criterion is fulfilled. The AOD values calculated in these layers (by use of lidar data) and correlation coefficients of their time variations with the dynamics of AOD of the total column (from satellite measurements) showed that the main bulk of atmospheric aerosol concentrated in the near-range transport, is localized in the layer from the ground to 3 km height. Though the situations when the bulk of aerosol is localized at the height of tropopause are also possible.

Time variations of AOD and chlorophyll "A" concentration were analyzed for two regions located along the northeast and east directions of the dust-storm aerosol transport. The analysis showed that high coefficients of correlation between local blooming and AOD increase were observed for both regions, caused by aerosol transport in the period of most intense outflow of aerosol from the Gobi dessert in 2006. This allow the conclusion to be drawn that atmospheric aerosol, transported to sea areas during strong sand storms in the Gobi, is one of the key factors influencing the development of phytoplankton communities in this region.

In this study we have presented only qualitative results on the influence of aerosol influx on phytoplankton communities and the corresponding approaches to study this influence with the use of satellite and lidar measurements. However, corresponding calibrations providing the development of algorithms for reconstructing chlorophyll "A" concentration from data of MODIS-Aqua and measurements of aerosol concentration, including its elemental composition, could enable one to study quantitative changes in the chlorophyll "A" concentration fields, their temporal dynamics characterizing the response of photosynthetic apparatus of phytoplankton cells to the income of mineral substances in the SLO.

Satellite data of the second level were granted from the NASA archives on the ocean color.[24]

References

1. D.J. Hofmann and J.M. Rosen, J. Geophys. Res. D **92**, No. 8, 9825–9830 (1987).

2. R.S. Stone, J.R. Key, and E.G. Dutton, J. Geophys. Res. Lett. **20**, No. 21, 2359–2362 (1993).

3. J. Williams, M. Reus, R. Krejci, and H. Fischer, Chem. Phys. Discuss. **2**, No. 1, 43–74 (2002).

4. D.V. Subba Rao, F. Al-Yaman, and C.V. Nageswara Rao, Naturwissenschaften **86**, No. 11, 525–529 (1999).

5. J.J. Walsh and K.A. Steidinger, J. Geophys. Res. C **106**, No. 6, 11597–11612 (2001).

6. J.K.B. Bishop, R.E. Davis, and J.T. Sherman, Science **298**, No. 5594, 817–821 (2002).

7. K.H. Coale, K.S. Johnson, S.E. Fitzwater, R.M. Gordon, S. Tanner, F.P. Chavez, L. Ferioli, C. Sakamoto, P. Rogers, F. Millero, P. Steinberg, P. Nightingale, D. Cooper, W.P. Cochlan, M.R. Landry, J. Constantinou, G. Rollwagen, A. Trasvina, and R. Kudela, Nature **383**, No. 6600, 495–501 (1996).

8. P.W. Boyd, A.J. Watson, C.S. Law, E.R. Abraham, T. Trull, R. Murdoch, D.C.E. Bakker, A.R. Bowie, K.O. Buesseler, H. Chang, M. Charette, P. Croot, K. Downing, R. Frew, M. Gall, M. Hadfield, J. Hall, M. Harvey, G. Jameson, J. LaRoche, M. Liddicoat, R. Ling, M.T. Maldonado, R.M. McKay, S. Nodder, S. Pickmere, R. Pridmore, S. Rintoul, K. Safi, Ph. Sutton, R. Strzepek, K. Tanneberger, S. Turner, A. Waite, and J. Zeldis, Nature **407**, No. 6805, 695–702 (2000).

9. http://www.cis-linet.basnet.by/

10. http://www-lidar.nies.go.jp/AsiaNet/

11. http://www.earlinet.org/

12. http://polder.cnes.fr

13. I. Uno, S. Satake, G.R. Carmichael, Y. Tang, Z. Wang, T. Takemura, N. Sugimoto, A. Shimizu, T. Murayama, T.A. Cahill, S. Cliff, M. Uematsu, S. Ohta, P.K. Quinn, and T.S. Bates, J. Geophys. Res. **109**. D19S24 (2004). doi:10.1029/2003JD004222.

14. http://weather.uwyo.edu/upperair/sounding.html

15. A.P. Chaikovskii, A.P. Ivanov, Yu.S. Balin, A.V. Elnikov, G.F. Tulinov, I.I. Plusnin, O.A. Bukin, and B.B. Chen, Atmos. Oceanic Opt. **18**, No. 12, 958–964 (2005).

16. A.Kh. Khrgian, *Atmospheric Physics* (Gidrometeoizdat, Leningrad, 1969), 670 pp.

17. http://cfors.ream.kyushu-u.ac.jp/

18. F. Marenco, V. Santacesaria, A.F. Bais, D. Balis, A. di Sarra, A. Papayannis, and C. Zerefos, Appl. Opt. **36**, No. 27, 6875–6886 (1997).

19. T. Takamura, Y. Sasano, and T. Hayasaka, Appl. Opt. **33**, 7132–7140 (1994).

20. V. Santacesaria, F. Marenco, D. Balis, A. Papayannis, and C. Zeferos, Il nuovo cimento. C **21**, No. 6, 585–596 (1998).

21. V.E. Zuev and G.M. Krekov, *Optical models of atmosphere* (Gidrometeoizdat, Leningrad, 1987), 254 pp.

22. D.A. Akmaikin, O.A. Bukin, M.S. Permyakov, and P.A. Saluk, in: *Modern problems of the remote sensing of Earth from space* (Poligrafservis, Moscow, 2005), V. 2. P. 64–69.

23. I. Lin, W.T. Liu, C.C. Wu, G.T.F. Wong, Ch. Hu, Zh. Chen, W.-D. Liang, Y. Yang, and K.-K. Liu, Geophys. Res. Lett. **30**, No. 13, 1718 (2003).

24. http://oceancolor.gsfc.nasa.gov/